

Theoretical Study of Adsorption Behavior of Dimethylamine and Ammonia on Al- and Ga-Doped BN Monolayer Surfaces Based on DFT

Zhengqin Cao, Changli Zhou, Jia Wang,* Gang Wei, Ting Li, and Kai Zhuang

Cite This: *ACS Omega* 2022, 7, 37857–37866

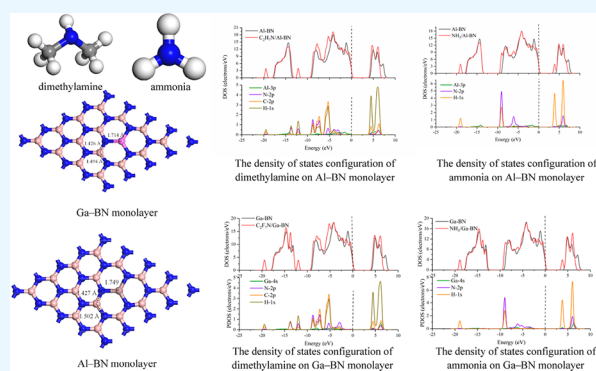
Read Online

ACCESS |

Metrics & More

Article Recommendations

ABSTRACT: Endogenous volatile organic compounds (VOCs) can reflect human health status and be used for clinical diagnosis and health monitoring. Dimethylamine and ammonia are the signature VOC gases of nephropathy. In order to find a potential gas sensitivity material for the detection of both signature VOC gases of nephropathy, this paper investigated the adsorption properties of dimethylamine and ammonia on Al- and Ga-doped BN monolayers based on density functional theory. Through analyzing the adsorption energy, adsorption distance, charge transfer, density of states, and HOMO/LUMO, the results indicated that the adsorption effect of Al- and Ga-doped BN monolayers to dimethylamine and ammonia is probably good, and these nanomaterials have the potential to be applied for nephropathy monitoring and clinical diagnosis.



1. INTRODUCTION

As an important physiological process of the human body, respiration is one of the ways for the human body to exchange substances with the environment.^{1–3} Relevant studies have shown that human exhaled gases contain thousands of volatile organic compounds (VOCs),⁴ among which endogenous VOCs can reflect human health status and be used for clinical diagnosis and health monitoring.^{5,6} For example, the concentration changes of ethane and other alkanes are related to lipid peroxidation.⁷ NO and CO can diagnose the presence of lung cancer.⁸ In addition, when the kidney is damaged or pathological changes occur, ammonium ions and urea cannot be metabolized and discharged from the kidney in time, resulting in an increase in the concentration of free ammonia, which will pass through the blood barrier in the form of ammonia and dimethylamine and exhale out of the human body. As a result, dimethylamine and ammonia are the signature VOC gases of nephropathy.⁹ The method of human health monitoring and clinical diagnosis based on exhaled gases has the advantages of being noninvasive and safe and allowing for fast sampling. However, the existing detection equipment has some disadvantages, such as complex structure, huge volume, high price, and so on. The detection of exhaled gases via a gas sensor can effectively reduce the cost and shorten the detection time. Therefore, a pressing task and challenge is to develop effective, low-cost, and gas sensitive material, as shown in Figure 1.

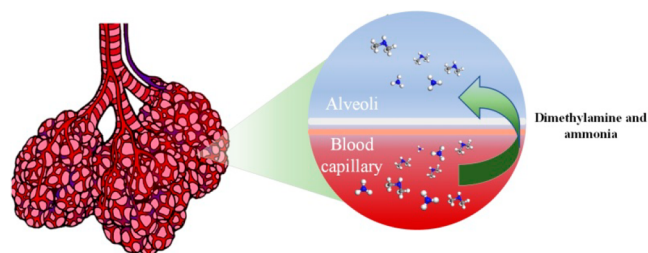


Figure 1. Landmark VOC gases of nephropathy.

Due to the strong responsivity and high sensitivity,^{10–13} boron nitride (BN) is a potential material for gas sensors. For example, Sajjad et al.¹⁴ explored the gas sensitivity of a boron nitride monolayer to CO₂, and Lin¹⁵ found that the h-BN monolayer has a fast response and excellent repeatability to ethanol and NH₃. Deng¹⁶ studied the adsorption of SO₂ on the (8, 0) boron nitride nanotube. In addition, atomic doping dramatically improves the gas sensitivity of intrinsic BN.^{17,18} Moreover, as the metallic congener of B, Al is more active, and

Received: August 4, 2022
Accepted: October 4, 2022
Published: October 14, 2022



the gas sensitivity is enhanced after doping Al on BN. Wang et al.¹⁹ modified the BN monolayer with Al for the ability to absorb CO₂. Peyghan et al.²⁰ developed Al-doped single walled BN nanotubes and found Al doping can notably enhance the adsorption energy of CO. Heidari et al.²¹ found an Al-doped h-BN monolayer is a potential material for adsorbing mercaptans.

Considering the above research, in this paper, the gas sensitivity of an Al-doped BN monolayer (Al–BN) to dimethylamine and ammonia was studied based on density functional theory (DFT). The work will guide the manufacture of a gas sensor and provide fundamental gas-sensitivity information of an Al-doped BN monolayer as a possible candidate for a resistance chemical sensor applied in nephropathy monitoring and clinical diagnosis.

2. COMPUTATION DETAILS

In this paper, all the quantum mechanics calculations were performed via the Dmol³ module^{22–24} based on DFT. The generalized gradient approximation (GGA) of the Perdew–Burke–Ernzerhof (PBE) functional was used to treat the electron exchange and correlation.^{25,26} The dual numerical plus polarization (DNP) basis set was adopted.^{27,28} The Brillouin zone was sampled as a 9 × 9 × 1 Monkhorst–Pack mesh k-point in geometric optimization. The DFT-D methods of Grimme were used to deal with the van der Waals interaction^{29,30} Maximum force, energy tolerance accuracy, and maximum atom displacement were selected as 0.002 Ha/Å, 1.0 × 10^{−5} Ha, and 5 × 10^{−3} Å, respectively.³¹ After a comparison, a 4 × 4 × 1 supercell with a 20 Å vacuum slab was built to avoid the interaction between two adjacent layers.

The adsorption energy E_{ad} represents the change of the gas molecules adsorption system, as shown in formula 1:^{32,33}

$$E_{ad} = E_{gas/Al-BN} - E_{gas} - E_{Al-BN} \quad (1)$$

in which $E_{gas/Al-BN}$ represents the total system energy after gas molecule adsorption, and E_{gas} and E_{Al-BN} represent the energy of the gas molecule and Al–BN monolayer, respectively.

The charge transfer $Q_{t-Hirshfeld}$ between the Al–BN monolayer and gas molecules is estimated via Hirshfeld analysis. If $Q_{t-Hirshfeld} < 0$, it denotes the electrons transfer from the Al–BN monolayer to gas molecules during the adsorption process. And the electrons transfer from gas molecules to the Al–BN monolayer when $Q_{t-Hirshfeld} > 0$.³⁴

3. RESULTS AND DISCUSSION

3.1. Optimization of the Al-Doped BN Monolayer, the Ga-Doped BN Monolayer, Dimethylamine, and Ammonia.

Due to the number of valence electrons of an Al atom being the same as that of a B atom but different from that of a N atom, there are no unpaired electrons after substituting B by Al; however, the electron deficiency after substituting N by Al will lead to the structural instability of a BN monolayer. In addition, the total formation energy of substituting B by Al (5.9951 eV) is much lower than that of substituting N by Al (14.6428 eV). Considering the above factors, we only simulated the situation that one B atom was substituted by Al. The optimized geometries of the BN and Al–BN monolayer are exhibited in Figure 2(a,b). It can be found that the length of the B–N bond is 1.445 Å, and six identical B–N bonds form a regular hexagon. Whereas, the geometric

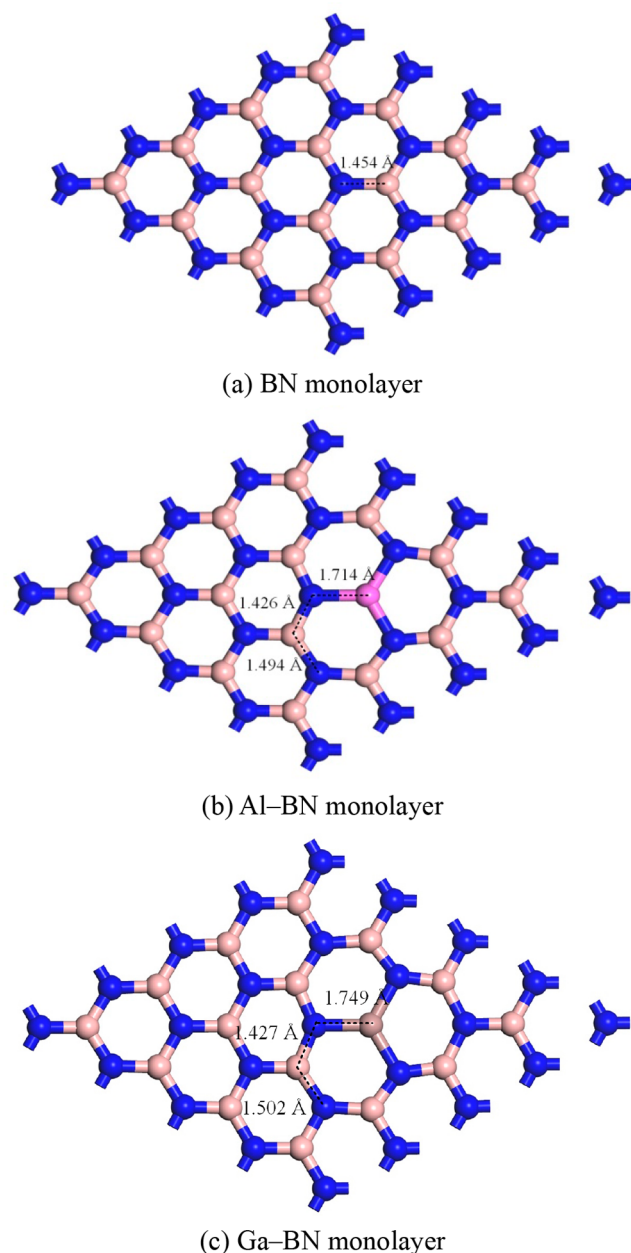


Figure 2. Optimized geometries of BN, Al–BN, and Ga–BN monolayers: (a) BN monolayer; (b) Al–BN monolayer; (c) Ga–BN monolayer.

configuration of the Al–BN monolayer is irregular around the Al atom. The lengths of Al–N and two adjacent B–N bonds are 1.714, 1.426, and 1.494 Å, respectively. The bandgap of the Al–BN monolayer only decreases 0.215 eV compared with that of the BN monolayer, as shown in Figure 3, which implies the doping of the Al atom has little effect on the electronic properties of the BN monolayer.

Due to Ga and Al being in the same chemical group, we also only simulated the situation that one B atom was substituted by Ga for a Ga-doped BN monolayer, and the optimized geometry of the Ga–BN monolayer is exhibited in Figure 2(c). One can observe that the lengths of Ga–N and two adjacent B–N bonds are 1.749, 1.427, and 1.502 Å, respectively. The bandgap of the Ga–BN monolayer decreases to 4.693 eV,

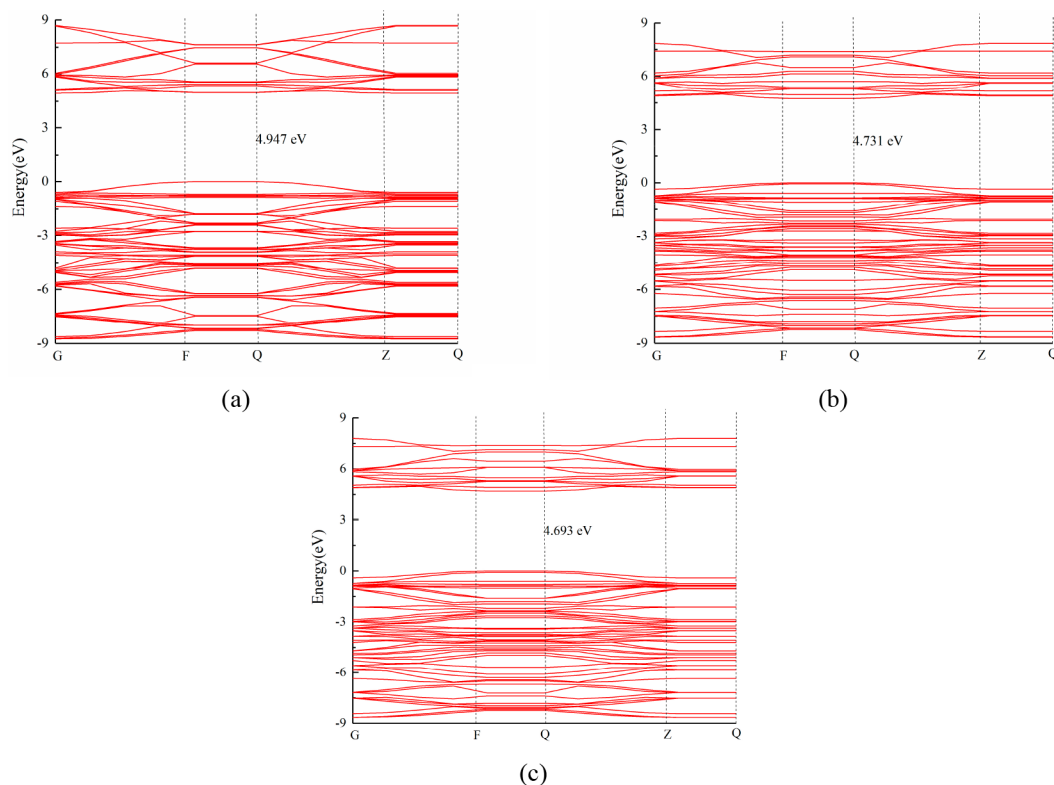


Figure 3. Band structures of BN, Al-BN, and Ga-BN monolayers: (a) BN monolayer; (b) Al-BN monolayer; (c) Ga-BN monolayer.

implying that the covalency of Ga-BN is greater than those of Bn and Al-BN monolayers.

In addition, there are 0.531 e electrons transferred from Al to adjacent N and 0.504 e electrons transferred from Ga to adjacent N, and they are quite more than the charge of 0.193 e transferring from B to adjacent N in an intrinsic BN monolayer according to Hirshfeld analysis.

The optimized geometry of dimethylamine, namely C_2H_7N , is shown in Figure 4(a). The lengths of the N-H bond, N-C bond, and C-H bond are 1.021, 1.466, and 1.100 Å, respectively. And the bond angles of H-C-H and N-C-H are 107.8 and 109.1°, respectively.

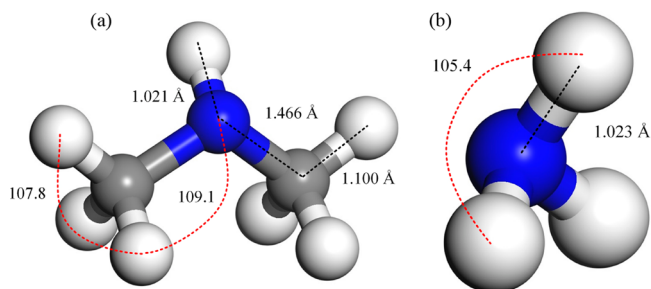


Figure 4. Optimized geometry of dimethylamine and ammonia: (a) dimethylamine; (b) ammonia.

The optimized geometry of ammonia, namely NH_3 , is exhibited in Figure 4(b). The length of N-H bonds is 1.023 Å. And the three bond angles of H-N-H are 105.4°.

3.2. Adsorption Properties of Dimethylamine on the Al-BN Monolayer. Considering the symmetry of the dimethylamine molecule, three initial adsorption modes are built. The M1 mode represents the N atom of dimethylamine

approaching the Al-BN monolayer. The M2 and M3 modes correspond to dimethylamine molecules approaching the Al-BN monolayer through the H atom connected to the C atom and the H atom connected to the N atom, respectively.

The optimized adsorption configurations and parameters of dimethylamine on the Al-BN monolayer are shown in Figure 5 and Table 1. Compared with M2 and M3 modes, the adsorption energies and charge transfer are closed to each other, but the adsorption distance of 3.493 Å in M2 mode is larger than that of 2.681 Å in M3 mode. In addition, the Al doping region of the monolayer concaves downward after adsorbing dimethylamine. As far as dimethylamine adsorbing on the Al-BN monolayer by M1 mode, a very different phenomenon has emerged. The Al doping region of the monolayer bulges upward after adsorption. The adsorption energy of -2.033 eV in M1 mode is the biggest in the three modes. The charge transfer in M1 mode increases to 0.345 e, which is 1 order of magnitude greater than those in M2 and M3 modes. The reason could be that a Lewis acid-base interaction arises, where dimethylamine is the Lewis base and the Al atom is the Lewis acid.³⁵ And the interaction between dimethylamine and Al-BN in M1 mode is probably chemisorption. Considering the above factors, the adsorption effect of the Al-BN monolayer to dimethylamine is probably good, and the most likely adsorption mode is M1 mode.

In order to further estimate the interaction mechanism between dimethylamine and the Al-BN monolayer, the total density of states (TDOS) and partial density of states (PDOS) distributions are discussed and exhibited in Figure 6. As for the TDOS configuration of M1 mode, there are two novel peaks appearing near -19 and -12 eV, and they are contributed by the C_2H_7N according to the PDOS. The conduct band region is dominated by the 1s orbital of H atoms of C_2H_7N . In addition, an impurity state appears near the conduct band

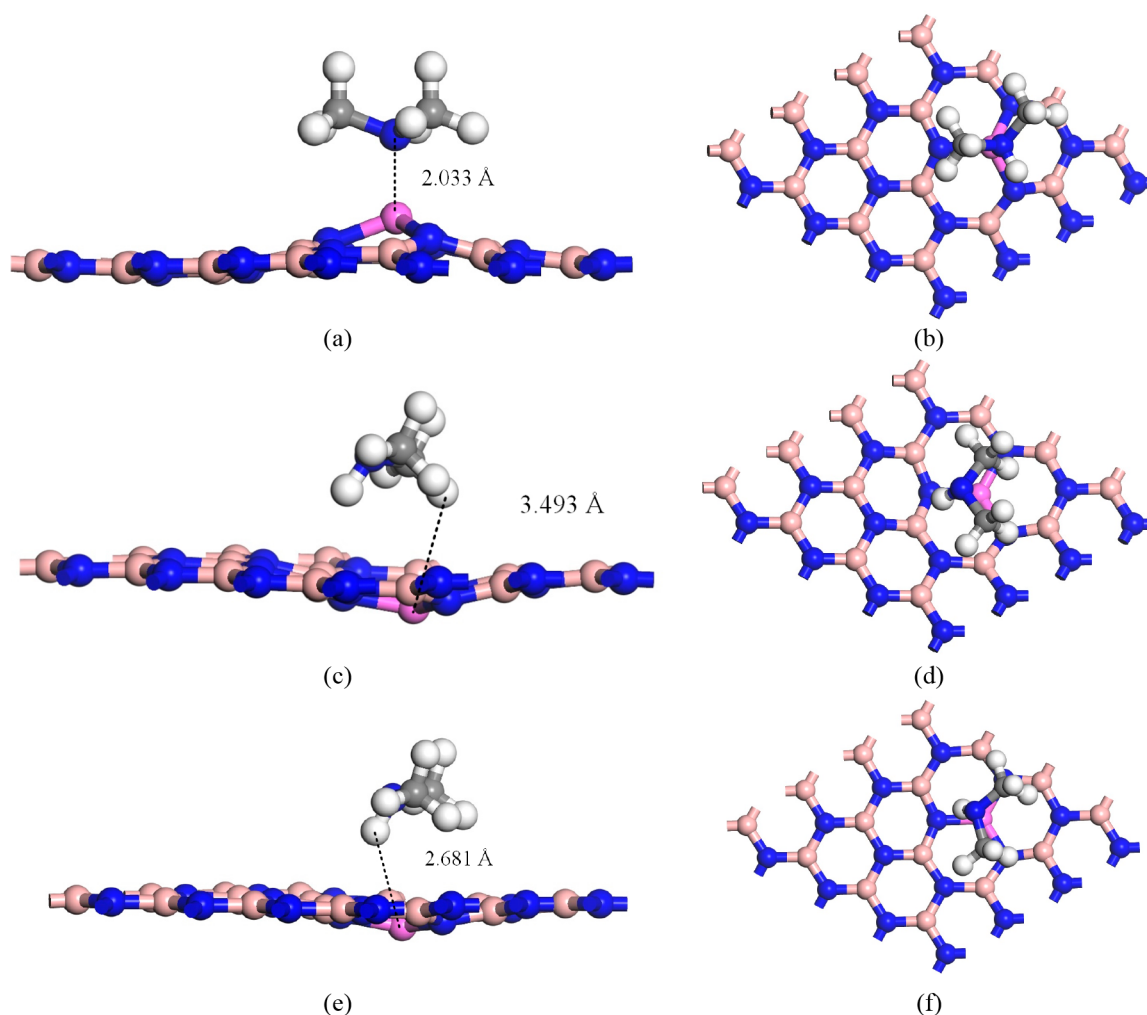


Figure 5. Adsorption configuration of dimethylamine on an Al–BN monolayer: (a) front view of M1 mode; (b) top view of M1 mode; (c) front view of M2 mode; (d) top view of M2 mode; (e) front view of M3 mode; (f) top view of M3 mode.

Table 1. Adsorption Parameters of Dimethylamine and Ammonia on an Al–BN Monolayer

Molecule	Configuration	E_{ad} (eV)	Distance (Å)	$Q_{\text{Hirshfeld}}$ (e)
Dimethylamine	M1	−2.113	2.033	0.345
	M2	−0.662	3.493	−0.036
	M3	−0.541	2.681	−0.043
Ammonia	N1	−2.125	2.043	0.354
	N2	−2.136	2.601	0.357

bottom, which is contributed by the 3p orbital of Al, the 2p orbital of N, the 2p orbital of C, and the 1s orbital of H.

The density of states configurations of M2 and M3 modes are shown in Figure 6(b,c). It can be found that there are two novel peaks appearing at −12.5 and −11 eV in the valence band region. The conduct band region is dominated by the 3p orbital of Al. Moreover, a novel peak appears in the Fermi level and is totally contributed by dimethylamine according to the PDOS, and there is no hybridization between the Al atom and dimethylamine. In addition, there is also a little bit of orbital hybridization among the orbital of Al and those orbitals of atoms of dimethylamine near the conduct band bottom and the valence band maximum. The coupling among the orbitals of Al, H, C and N atoms in the impurity state near the conduct band bottom provides another theoretical support that a strong

interaction occurred between Al–BN and dimethylamine by M1 mode with a strong charge transfer process, which probably leads the change of conductivity of such monolayer after dimethylamine.³⁶

The distributions of the lowest unoccupied molecular orbital (LUMO) and highest occupied molecular orbital (HOMO) for the Al–BN monolayer and dimethylamine adsorbing on Al–BN monolayer are exhibited in Figures 7 and 8, respectively. The energy gap E_g is shown in formula 2:

$$E_g = E_{LUMO} - E_{HOMO} \quad (2)$$

Where, E_{LUMO} and E_{HOMO} represent the values of the LUMO and HOMO, respectively.

It can be observed that the distributions of the LUMO and HOMO become very uneven after dimethylamine adsorbs on the Al–BN monolayer. The energy gap decreases to 0.180 eV in M1 mode, an indication that the chemical activity of Al–BN will be significantly increased.²⁰ The LUMO is mainly distributed on the dimethylamine molecule, and the HOMO is mainly distributed on the Al–BN monolayer. However, the LUMO is mainly distributed on the Al–BN monolayer, and the HOMO is mainly distributed on the dimethylamine molecule in M2 mode. In addition, compared with those of Al–BN, the LUMO decreases to −0.065 eV and the HOMO increases to −0.190 eV in M2 mode. As a result, the energy

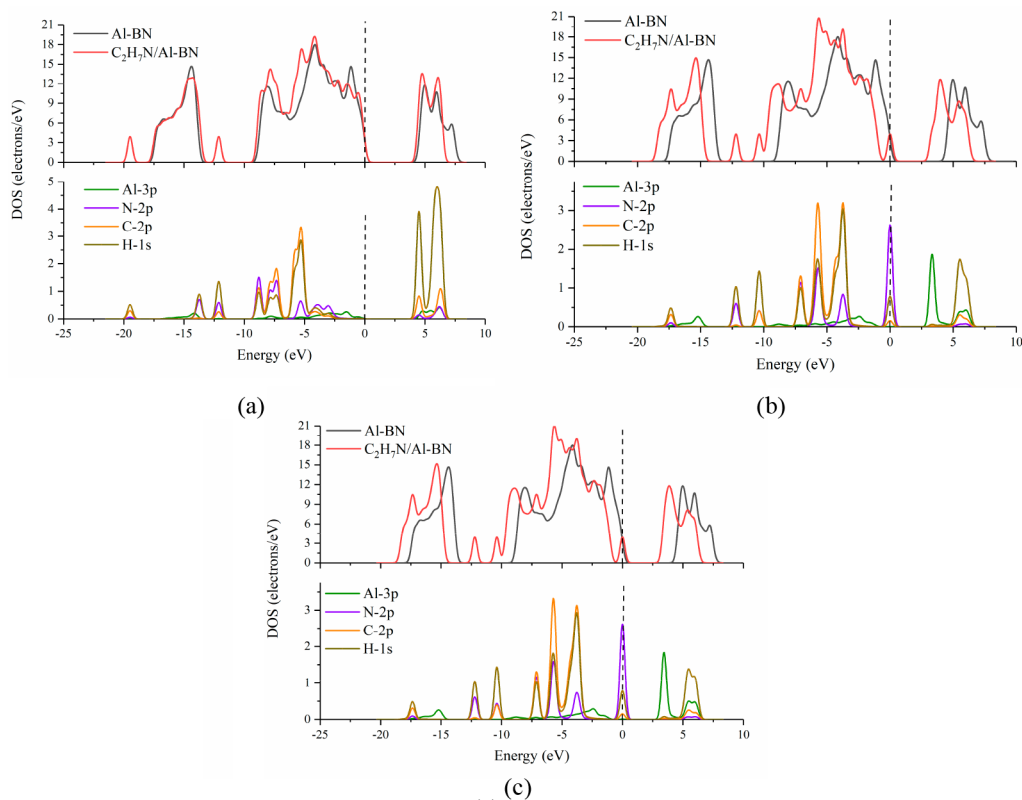


Figure 6. Density of states configuration of dimethylamine on an Al–BN monolayer: (a) M1 mode; (b) M2 mode; (c) M3 mode

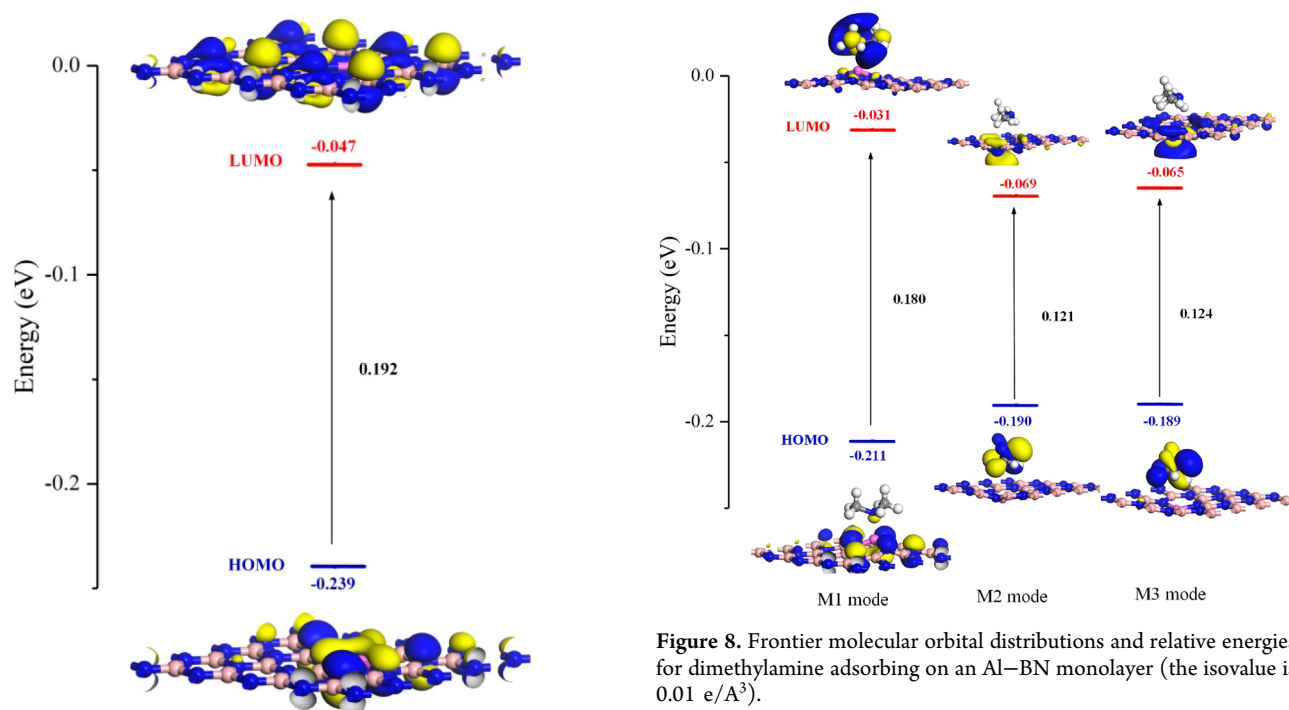


Figure 7. Frontier molecular orbital distributions and relative energies for the Al–BN monolayer (the isovalue is $0.01 \text{ e}/\text{Å}^3$).

gap decreases about 37% to 0.121 eV. The distribution of LUMO and HOMO in M3 mode is similar to that in M2 mode. Due to the smaller energy gap, electrons are easier to transfer from the HOMO to LUMO in M2 and M3 modes

Figure 8. Frontier molecular orbital distributions and relative energies for dimethylamine adsorbing on an Al–BN monolayer (the isovalue is $0.01 \text{ e}/\text{Å}^3$).

than in M1 mode, indicating M2 and M3 modes are more unstable than M1 mode.

3.3. Adsorption Properties of Ammonia on the Al–BN Monolayer. For ammonia adsorbing on the Al–BN monolayer, two initial adsorption modes are considered. The N1 mode represents the N atom of ammonia approaching the Al–BN monolayer, and the N2 mode represents the H atom of ammonia approaching the Al–BN monolayer. The optimized

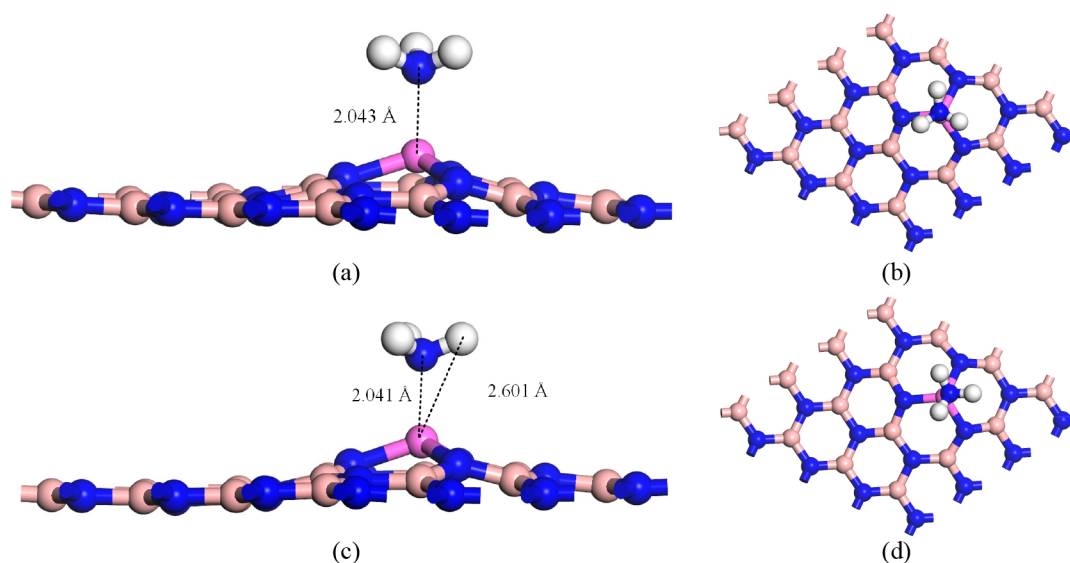


Figure 9. Adsorption configuration of ammonia on an Al–BN monolayer: (a) front view of N1 mode; (b) top view of N1 mode; (c) front view of N2 mode; (d) top view of N2 mode.

adsorption configurations of N1 are shown in Figure 9(a,b). The adsorption distance and adsorption energy are 2.043 Å and -2.125 eV, respectively. The charge transfer of 0.354 e is quite large, which indicates that a Lewis acid–base interaction probably happens during adsorption. In addition, the Al doping region of the monolayer bulges upward after adsorption of ammonia, and the three N–H bonds change to 1.025, 1.025, and 1.026 Å, respectively.

The optimized adsorption configurations of N2 are exhibited in Figure 9(c,d). It is intriguing that the closest distance of 2.041 Å between the adsorbate and adsorbent is from the N atom of ammonia to the Al atom of the Al–BN monolayer, shorter than the value we set initially and closer to that of N1 mode. However, H atoms gradually move away from the monolayer during the adsorption process, and the final optimized distance between H atom of ammonia to Al atom of Al–BN increases to 2.601 Å. In addition, the values of energy and charge transfer also approximately equal to those of N1 mode. In a word, the optimized adsorption configuration of N2 mode is almost the same as those of N1 mode. From those, we can conclude that there could be a strong chemisorption interaction between ammonia and the Al–BN monolayer, and the most likely adsorption mode is N1 mode.

Due to the optimized adsorption configuration of N2 mode being almost the same as that of N1 mode, we only discuss the DOS configuration of N1 mode, and it is exhibited in Figure 10. One novel peak appears in the valence band region, mainly being contributed by the 1s orbital of H atom. The conduct band region is dominated by the 1s orbital of H atoms of NH_3 , and the conduct band minimum is smaller after ammonia adsorption, which leads to the pseudogap decrease and further results in the increase of the conductivity of Al–BN.

The distributions of LUMO and HOMO for ammonia adsorbing on the Al–BN monolayer are exhibited in Figure 11. The values of LUMO and HOMO are -0.052 and -0.211 eV, respectively. Compared with those of the Al–BN monolayer, the LUMO decreases to -0.052 eV, but the HOMO increases to -0.211 eV after ammonia adsorbs on the Al–BN monolayer. As a consequence, the energy gap decreases to 0.159 eV. In addition, the LUMO is mainly distributed on the

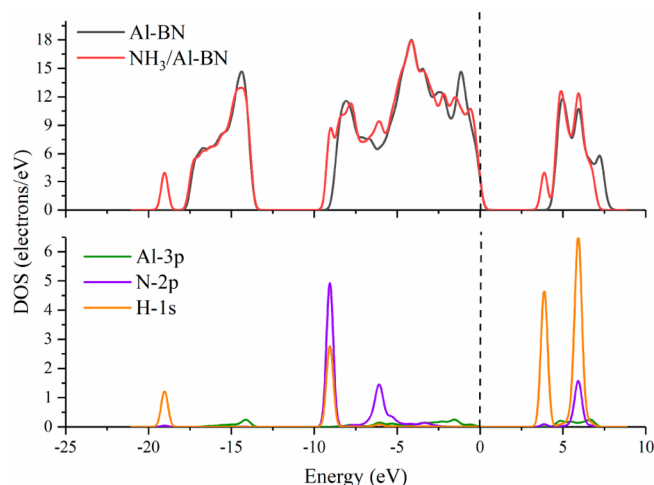


Figure 10. Density of states configuration of ammonia on an Al–BN monolayer by the N1 mode.

ammonia molecule, whereas HOMO is mainly distributed on the Al–BN monolayer.

3.4. Adsorption Properties of Dimethylamine and Ammonia on the Ga–BN Monolayer. Considering the number of valence electrons of a Ga atom is the same as that of an Al atom and both the most likely adsorption modes for dimethylamine and ammonia on Al-doped BN monolayer are the N atom of dimethylamine and ammonia approaching the Al–BN monolayer, we only consider the N atom of dimethylamine and ammonia approaching the Ga–BN monolayer as well.

The optimized adsorption configurations of dimethylamine and ammonia are exhibited in Figure 12, and the adsorption parameters are shown in Table 2. It is intriguing that both the adsorption energies of -1.975 eV for dimethylamine and -1.653 eV for ammonia are smaller for absorbing on Ga–BN than when adsorbing on Al–BN. The charge transfers of 0.314 e for dimethylamine and 0.323 e for ammonia when adsorbing on Ga–BN are a little smaller than the charge transfer when adsorbing on Al–BN as well. Dimethylamine and ammonia act

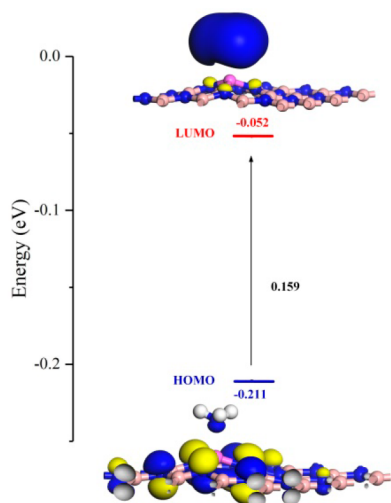


Figure 11. Frontier molecular orbital distributions and relative energies for ammonia adsorbing on an Al-BN monolayer (the isovalue is $0.01 \text{ e}/\text{\AA}^3$).

as a Lewis base and the Ga atom acts as a Lewis acid in the adsorption process. However, all the adsorption distances are closed to 2.00 \AA , and the Ga doping region of monolayer bulges upward after dimethylamine and ammonia adsorption. The adsorption parameters also indicate that there are strong interactions occurring between the Ga-BN monolayer and dimethylamine or ammonia, respectively.

The TDOS and PDOS distributions are exhibited in Figure 13 to estimate the interaction mechanism between dimethylamine, ammonia, and the Al-BN monolayer, respectively. As for dimethylamine, there is one novel peak appearing in the valence band region, which is contributed by $\text{C}_2\text{H}_7\text{N}$ via the analysis of PDOS. The strong adsorption interaction between $\text{C}_2\text{H}_7\text{N}$ and the Ga-BN monolayer can be reflected by the

Table 2. Adsorption Parameters of Dimethylamine and Ammonia on a Ga-BN Monolayer

Molecule	E_{ad} (eV)	Distance (\AA)	$Q_{t\text{-Hirshfeld}}$ (e)
$\text{C}_2\text{H}_7\text{N}$	-1.975	2.090	0.314
NH_3	-1.652	2.129	0.323

orbital hybridization near the conduction band minimum (CBM), where the 2p orbital of N atom, the 2p orbital of the C atom, and the 1s orbital of the H atom of the $\text{C}_2\text{H}_7\text{N}$ molecule are coupled with the 4s orbital of the Ga atom of the Ga-BN monolayer. As for ammonia, it can be found that one novel peak appears in the conduction band region due to the 1s orbital of H atom of NH_3 and it is hybridized with the 4s orbital of the Ga atom. The DOS in the Fermi level does not change after NH_3 adsorption. The DOS distributions are also the strong interaction between the two kinds of the signature VOC gases of nephropathy and Ga-BN monolayer.

The distributions of the LUMO and HOMO for Ga-BN monolayer, dimethylamine, and ammonia adsorbing on the Ga-BN monolayer are exhibited in Figure 14. It could be found that the values and distributions of the LUMO and HOMO change significantly after dimethylamine and ammonia adsorption. The LUMO is more localized on the dimethylamine and ammonia. Due to the energy gaps decreasing much from 0.195 to 0.180 and 0.156 eV, respectively, the chemical activity of such systems will be significantly increased. In addition, the values of the LUMO and HOMO are -0.030 and -0.210 eV, respectively, for dimethylamine adsorbing on Ga-BN. Compared with dimethylamine adsorbing on the Al-BN monolayer, both of the values of the LUMO and HOMO increase 0.001 eV. As a consequence, the energy gap is also 0.180 eV. As for ammonia, the values of LUMO and HOMO are -0.053 and -0.209 eV, respectively. Comparing with ammonia adsorbing on the Al-BN monolayer, the energy gap decreases a little to 0.156 eV.

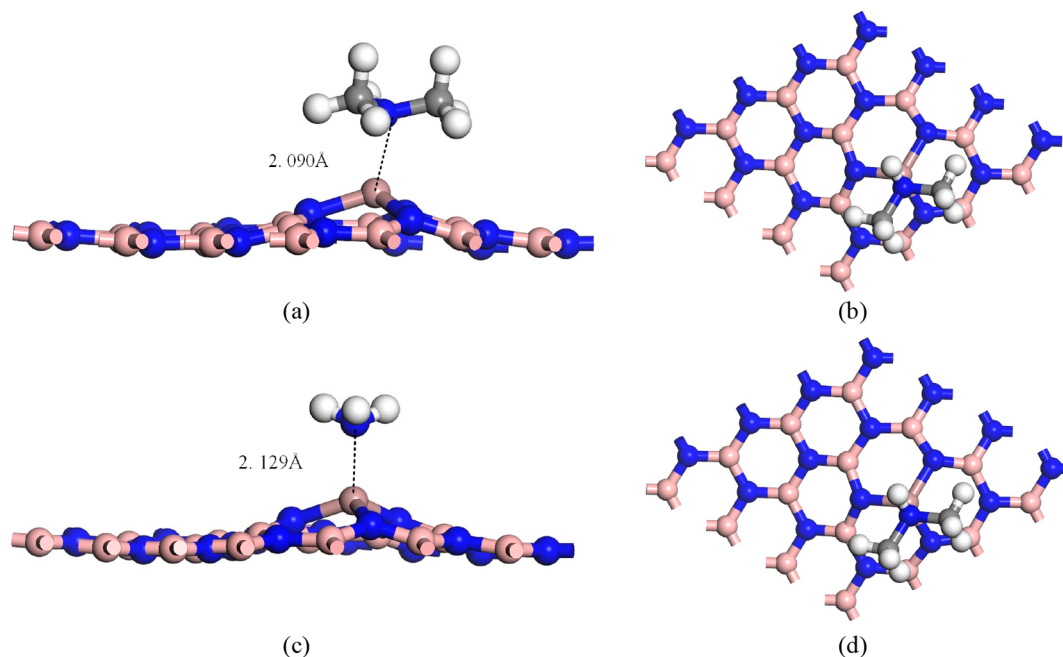


Figure 12. Adsorption configuration of ammonia on a Ga-BN monolayer: (a) front view of $\text{C}_2\text{H}_7\text{N}$; (b) top view of $\text{C}_2\text{H}_7\text{N}$; (c) front view of NH_3 ; (d) top view of NH_3

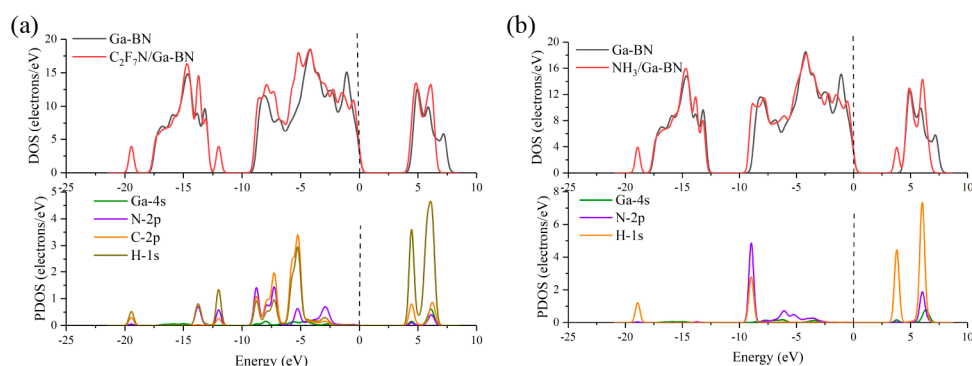


Figure 13. Density of states configuration of dimethylamine and ammonia on a Ga–BN monolayer: (a) dimethylamine; (b) ammonia.

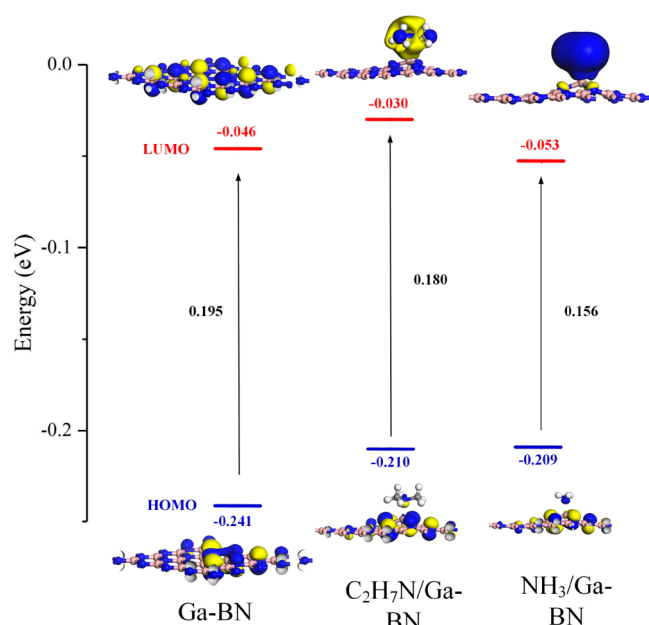


Figure 14. Frontier molecular orbital distributions and relative energies for a Ga–BN monolayer as well as dimethylamine and ammonia adsorbing on a Ga–BN monolayer (the isovalue is $0.01 \text{ e}/\text{\AA}^3$)

Currently, the quantum mechanics calculation study on the surface adsorption of dimethylamine has not been reported yet; however, there are many reports about surface adsorption of ammonia. And the adsorption parameters of ammonia on several kinds of adsorbents are shown in Table 3. The adsorption energies and electronic properties of ammonia adsorbing on the Al- and Ga-BN are significantly higher compared to those reported^{37–41} for it adsorbing on pristine

Table 3. Adsorption Parameters of Ammonia on Different Adsorbents

Adsorbents	E_{ad} (eV)	Distance (Å)	Q_t (e)
Graphyne oxide ³⁷	−0.382	2.994	−0.016 (Hirshfeld)
Ni-doped graphyne ³⁸	2.389	—	—
Si-doped graphyne ³⁸	1.704	—	—
TiO ₂ (100) ³⁹	1.075	2.238	—
BC ₃ ⁴⁰	−1.45	1.67	0.610 (Mulliken)
WO ₃ (001) surface-supported Au ⁴¹	−1.43	2.310	−0.13 (Mulliken)

graphene, and it is also comparable to the reported adsorption energy of ammonia on Ni-doped graphyne.³⁸

4. CONCLUSIONS

In order to find a potential gas sensitivity material for the detection of nephropathy's signature VOC gases, namely dimethylamine and ammonia, the adsorption properties of dimethylamine and ammonia on Al- and Ga-doped BN monolayers are comprehensively investigated based on DFT. The conclusions are summarized:

- (1) The process of dimethylamine adsorbing on a Al–BN monolayer is exothermic, and the most likely adsorption mode is the M1 mode (the N atom of dimethylamine approaching the Al–BN monolayer). And there could be chemisorption between dimethylamine and the Al–BN monolayer because of the large adsorption energy, the large amount of charge transfer, and the short adsorption distance.
- (2) The most likely adsorption mode for ammonia on an Al-doped BN monolayer is N1 mode (the N atom of ammonia approaching the Al–BN monolayer). There is also a strong chemical interaction between ammonia and the Al–BN monolayer.
- (3) The adsorption parameters of dimethylamine and ammonia on the Ga-doped BN monolayer are close to those on the Al-doped BN monolayer. And the adsorption effect of the Ga–BN monolayer to dimethylamine and ammonia is probably good as well.

AUTHOR INFORMATION

Corresponding Author

Jia Wang – College of medical informatics, Chongqing Medical University, Chongqing 400016, China; orcid.org/0000-0002-2928-7186; Email: 102509@cqmu.edu.cn

Authors

Zhengqin Cao – College of Electrical Engineering, Chongqing University of Science and Technology, Chongqing 401331, China; orcid.org/0000-0002-8274-629X

Changli Zhou – College of Electrical Engineering, Chongqing University of Science and Technology, Chongqing 401331, China

Gang Wei – College of Electrical Engineering, Chongqing University of Science and Technology, Chongqing 401331, China; orcid.org/0000-0003-2182-8635

Ting Li – Traditional Chinese medicine hospital of Jiulongpo district in Chongqing, Chongqing 400050, China

Kai Zhuang – College of Electrical Engineering, Chongqing University of Science and Technology, Chongqing 401331, China

Complete contact information is available at:
<https://pubs.acs.org/10.1021/acsomega.2c04963>

Notes

The authors declare no competing financial interest.

ACKNOWLEDGMENTS

This work was supported in part by the Science and Technology Research Program of Chongqing Municipal Education Commission (Grant No. KJQN202001524, KJQN-K202100434, KJQN-201901543), the Chongqing Natural Science Foundation (Grant No. cstc2020cyj-msxmX0267), and the Intelligent Medicine Program of Chongqing Medical University (Grant No. ZHYX202120).

REFERENCES

- (1) Kim, K. H.; Jahan, S. A.; Kabir, E. A review of breath analysis for diagnosis of human health. *TrAC, Trends Anal. Chem.* **2012**, *33*, 1–8.
- (2) Pleil, J. D.; Lindstrom, A. B. Exhaled human breath measurement method for assessing exposure to halogenated volatile organic compounds. *Clin. Chem.* **1997**, *43*, 723–730.
- (3) Montesantos, S.; Katz, I.; Venegas, J.; Pichelin, M.; Caillibotte, G. The effect of disease and respiration on airway shape in patients with moderate persistent asthma. *PLoS One* **2017**, *12*, No. e0182052.
- (4) Nakhleh, M. K.; Amal, H.; Jeries, R.; Broza, Y. Y.; Aboud, M.; Gharra, A.; Ivgi, H.; Khatib, S.; Badarneh, S.; Har-Shai, L.; et al. Diagnosis and classification of 17 diseases from 1404 subjects via pattern analysis of exhaled molecules. *ACS Nano* **2017**, *11*, 112–125.
- (5) Purkhart, R.; Kohler, H.; Liebler-Tenorio, E.; Meyer, M.; Becher, G.; Kikowatz, A.; Reinhold, P. Chronic intestinal Mycobacteria infection: discrimination via VOC analysis in exhaled breath and headspace of feces using differential ion mobility spectrometry. *J. Breath Res.* **2011**, *5*, 027103.
- (6) Monedeiro, F.; dos Reis, R. B.; Peria, F. M.; Sares, C. T. G.; De Martinis, B. S. Investigation of sweat VOC profiles in assessment of cancer biomarkers using HS-GC-MS. *J. Breath Res.* **2020**, *14*, 026009.
- (7) Skeldon, K. D.; McMillan, L. C.; Wyse, C. A.; Monk, S. D.; Gibson, G.; Patterson, C.; France, T.; Longbottom, C.; Padgett, M. J. Application of laser spectroscopy for measurement of exhaled ethane in patients with lung cancer. *Respir. Med.* **2006**, *100*, 300–306.
- (8) Tisch, U.; Haick, H. Chemical sensors for breath gas analysis: the latest developments at the Breath Analysis Summit. 2013. *J. Breath Res.* **2014**, *8*, 027103.
- (9) Libardoni, M.; Stevens, P. T.; Waite, J. H.; Sacks, R. Analysis of human breath samples with a multi-bed sorption trap and comprehensive two-dimensional gas chromatography (GC × GC). *J. Chromatogr. B* **2006**, *842*, 13–21.
- (10) Li, J.; He, S.; Li, R.; Dai, W.; Tao, J.; Wang, C.; Liu, J.; Wu, T.; Tang, C. Template-free synthesis of three dimensional porous boron nitride nanosheets for efficient water cleaning. *RSC Adv.* **2018**, *8*, 32886–32892.
- (11) Luan, X.; Yu, R.; Zhang, Q.; Zhang, S.; Cheng, L. Boron nitride coating of sapphire optical fiber for high temperature sensing applications. *Surf. Coat. Technol.* **2019**, *363*, 203–209.
- (12) Glavin, N. R.; Waite, A. R.; Muratore, C.; Bultman, J. E.; Hu, J.; Gengler, J. J.; Voevodin, A. A.; Fisher, T. S. Thermal conductance at nanoscale amorphous boron nitride/metal interfaces. *Surf. Coat. Technol.* **2020**, *397*, 126017.
- (13) Satyanarayana, L.; Gopal Reddy, C. V.; Manorama, S. V.; Rao, V. J. liquid-petroleum-gas sensor based on a spinel semiconductor, znga 2 o 41. *Sens. Actuators. B* **1998**, *46*, 1–7.
- (14) Sajjad, M.; Feng, P. Study the gas sensing properties of boron nitride nan osheets. *Mater. Res. Bull.* **2014**, *49*, 35–38.
- (15) Lin, L.; Liu, T.; Zhang, Y.; Sun, R.; Zeng, W.; Wang, Z. Synthesis of boron nitride nanosheets with a few atomic layers and their gas-sensing performance. *Ceram. Int.* **2016**, *42*, 971–975.
- (16) Deng, Z. Y.; Zhang, J. M.; Xu, K. W. Adsorption of SO₂ molecule on doped (8, 0) boron nitride nanotube: A first-principles study. *Physica. E (Amsterdam, Neth.)* **2016**, *76*, 47–51.
- (17) Baei, M. T.; Kanani, Y.; Rezaei, V. J.; Soltani, A. Adsorption phenomena of gas molecules upon Ga-doped BN nanotubes: A DFT study. *Appl. Surf. Sci.* **2014**, *295*, 18–25.
- (18) Ma, S. Q. Gas Sensitivity of Cr Doped BN Sheets. *Appl. Mech. Mater.* **2015**, *799–800*, 166–170.
- (19) Wang, G. Y.; Zheng, K.; Huang, Y. X.; Yu, J.; Wu, H.; Chen, X.; Tao, L.-Q. An investigation of the positive effects of doping an Al atom on the adsorption of CO₂ on BN nanosheets: a DFT study. *Phys. Chem. Chem. Phys.* **2020**, *22*, 9368–9374.
- (20) Peyghan, A. A.; Soltani, A.; Pahlevani, A. A.; Kanani, Y.; Khajeh, S. A first-principles study of the adsorption behavior of CO on Al- and Ga-doped single-walled BN nanotubes. *Appl. Surf. Sci.* **2013**, *270*, 25–32.
- (21) Heidari, H.; Afshari, S.; Habibi, E. Sensing properties of pristine, Al-doped, and defected boron nitride nanosheet toward mercaptans: a first-principles study. *RSC Adv.* **2015**, *5*, 94201–94209.
- (22) Delley, B. J. From molecules to solids with the DMol3 approach. *J. Chem. Phys.* **2000**, *113*, 7756–7764.
- (23) Cao, Z.; Wei, G.; Zhang, H.; Hu, D.; Yao, Q. Adsorption Property of CS₂ and COF₂ on Nitrogen-Doped Anatase TiO₂ (101) Surfaces: A DFT Study. *ACS Omega* **2020**, *5*, 21662–21668.
- (24) Liu, Z.; Gui, Y.; Xu, L.; Chen, X. Adsorption and sensing performances of transition metal (Ag, Pd, Pt, Rh, and Ru) modified WSe₂ monolayer upon SF₆ decomposition gases (SOF₂ and SO₂F₂). *Appl. Surf. Sci.* **2022**, *581*, 152365.
- (25) Gui, Y.; Shi, J.; Yang, P.; Li, T.; Tang, C.; Xu, L. Platinum modified MoS₂ monolayer for adsorption and gas sensing of SF₆ decomposition products: a DFT study. *High Voltage* **2020**, *5*, 454–462.
- (26) Gui, Y.; Liu, Z.; Ji, C.; Xu, L.; Chen, X. Adsorption behavior of metal oxides (CuO, NiO, Ag₂O) modified GeSe monolayer towards dissolved gases (CO, CH₄, C₂H₂, C₂H₄) in transformer oil. *J. Ind. Eng. Chem.* **2022**, *112*, 134–145.
- (27) Chen, D.; Zhang, X.; Tang, J.; Cui, H.; Li, Y.; Zhang, G.; Yang, J. Density functional theory study of small Ag cluster adsorbed on graphyne. *Appl. Surf. Sci.* **2019**, *465*, 93–102.
- (28) Zheng, W.; Tang, C.; Xie, J.; Gui, Y. Micro-scale effects of nano-SiO₂ modification with silane coupling agents on the cellulose/nano-SiO₂ interface. *Nanotechnology* **2019**, *30*, 445701.
- (29) Grimme, S. Semiempirical GGA-type density functional constructed with a long-range dispersion correction. *J. Comput. Chem.* **2006**, *27*, 1787–1799.
- (30) Liu, Y.; Zhao, J.; Li, F.; Chen, Z. Appropriate description of intermolecular interactions in the methane hydrates: An assessment of DFT methods. *J. Comput. Chem.* **2013**, *34*, 121–131.
- (31) Zhang, X.; Yu, L.; Tie, J.; Dong, X. Gas Sensitivity and Sensing Mechanism Studies on Au-Doped TiO₂ Nanotube Arrays for Detecting SF₆ Decomposed Components. *Sensors* **2014**, *14*, 19517–19532.
- (32) Chen, W. L.; Gui, Y. G.; Li, T.; Zeng, H.; Xu, L.; Ding, Z. Y. Gas-sensing properties and mechanism of Pd-GaNNTs for air decomposition products in ring main unit. *Appl. Surf. Sci.* **2020**, *531*, 147293.
- (33) Xiao, S.; Zhang, J.; Zhang, X.; Cui, H. Pt-doped single-walled CNT as a superior media for evaluating the operation status of insulation devices: A first-principle study. *AIP Adv.* **2018**, *8*, 105101.
- (34) Gui, Y.; Shi, J.; Yang, P.; Li, T.; Tang, C.; Xu, L. Platinum modified MoS₂ monolayer for adsorption and gas sensing of SF₆ decomposition products: a DFT study. *High Voltage* **2020**, *5*, 454.
- (35) Molani, F.; Jalili, S.; Schofield, J. Al-doped B80 fullerene as a suitable candidate for H₂, CH₄, and CO₂ adsorption for clean energy applications. *J. Saudi Chem. Soc.* **2018**, *22*, 49–57.

(36) Li, S.; Zhu, S.; Zhou, Q.; Gui, Y.; Wei, X. Adsorption mechanism of decomposition gas of SF₆ circuit breaker on MOF-505 analogue. *Vacuum* **2021**, *183*, 109816.

(37) Mofidi, F.; Reisi-Vanani, A. Investigation of the electronic and structural properties of graphyne oxide toward CO, CO₂ and NH₃ adsorption: A DFT and MD study. *Appl. Surf. Sci.* **2020**, *507*, 145134.

(38) Peyghan, A. A.; Rastegar, S. F.; Hadipour, N. L. DFT study of NH₃ adsorption on pristine, Ni- and Si-doped graphynes. *Phys. Lett. A* **2014**, *378*, 2184–2190.

(39) Guo, X. J.; Liu, W.; Fang, W.; Cai, L.; Zhu, Y.; Lu, L.; Lu, X. DFT study of coverage-dependend adsorption of NH₃ on TiO₂-B (100) surface. *Phys. Chem. Chem. Phys.* **2012**, *14*, 16618–16625.

(40) Mehdi Aghaei, S.; Monshi, M.M.; Torres, I.; Zeidi, S.M.J.; Calizo, I. DFT study of adsorption behavior of NO, CO, NO₂, and NH₃ molecules on graphene-like BC₃: A search for highly sensitive molecular sensor. *Appl. Surf. Sci.* **2018**, *427*, 326–333.

(41) Lin, L.; Huang, J.; Yu, W.; He, C.; Tao, H.; Xu, Y.; Zhu, L.; Wang, P.; Zhang, Z. A periodic DFT study on adsorption of small molecules (CH₄, CO, H₂O, H₂S, NH₃) on the WO₃ (001) surface-supported Au. *Commun. Theor. Phys.* **2020**, *72*, 035501.